crystals

MDPI

Article

Influence of HAP on the Morpho-Structural Properties and Corrosion Resistance of ZrO_2-Based Composites for Biomedical Applications

Réka Barabás [1], Carmen Ioana Fort [2], Graziella Liana Turdean [2,*] and Liliana Bizo [2,*]

[1] Department of Chemistry and Chemical Engineering of Hungarian Line of Study, Faculty of Chemistry and Chemical Engineering, Babeş-Bolyai University, 11 Arany Janos Street, RO-400028 Cluj-Napoca, Romania; reka.barabas@ubbcluj.ro

[2] Department of Chemical Engineering, Faculty of Chemistry and Chemical Engineering, Babeş-Bolyai University, 11 Arany Janos Street, RO-400028 Cluj-Napoca, Romania; ioana.fort@ubbcluj.ro

* Correspondence: graziella.turdean@ubbcluj.ro (G.L.T.); liliana.bizo@ubbcluj.ro (L.B.)

Abstract: In the present work, ZrO_2-based composites were prepared by adding different amounts of antibacterial magnesium oxide and bioactive and biocompatible hydroxyapatite (HAP) to the inert zirconia. The composites were synthesized by the conventional ceramic processing route and morpho-structurally analyzed by X-ray powder diffraction (XRPD) and scanning electron microscopy/energy dispersive X-ray spectroscopy (SEM/EDS). Two metallic dental alloys (i.e., Ni–Cr and Co–Cr) coated with a chitosan (Chit) membrane containing the prepared composites were exposed to aerated artificial saliva solutions of different pHs (i.e., 4.3, 5, 6) and the corrosion resistances were investigated by electrochemical impedance spectroscopy technique. The obtained results using the two investigated metallic dental alloys shown quasi-similar anticorrosive properties, having quasi-similar charge transfer resistance, when coated with different ZrO_2-based composites. This behavior could be explained by the synergetic effect between the diffusion process through the Chit-composite layer and the roughness of the metallic electrode surface.

Keywords: zirconia; hydroxyapatite; X-ray powder diffraction; scanning electron microscopy/energy dispersive X-ray spectroscopy; electrochemical impedance spectroscopy

Citation: Barabás, R.; Fort, C.I.; Turdean, G.L.; Bizo, L. Influence of HAP on the Morpho-Structural Properties and Corrosion Resistance of ZrO_2-Based Composites for Biomedical Applications. *Crystals* **2021**, *11*, 202. https://doi.org/10.3390/cryst11020202

Academic Editor: Michele Iafisco
Received: 17 December 2020
Accepted: 12 February 2021
Published: 19 February 2021

1. Introduction

Beside many biomaterials, hydroxyapatite (HAP), with chemical formula $Ca_{10}(PO_4)_6(OH)_2$, continue to be extensively studied, being bioactive, highly osteoconductive, with high strength and modulus of elasticity, and high biocompatibility [1–3]. From the point of view of biocompatibility, it is a calcium phosphate (CaP) bioceramic similar to the human hard tissues in morphology and composition and seems to be the most suitable ceramic material for hard tissue replacement implants. Thermodynamically, HAP it is the most stable CaP compound under physiological conditions as pH, temperature, and composition of the body fluids. HAP ceramics does not exhibit any cytotoxic effects, shows excellent biocompatibility with hard tissues and also with skin and muscle tissues and can directly bond to the bone [4,5]. However, HAP presents some disadvantages, such as brittleness, low tensile strength and fracture toughness. Consequently, these disadvantages resulted in the limitation of usage for example in load-bearing orthopaedic implants. In the last years, there has been a lot of research aiming to fabricate more mechanically reliable bioactive ceramics, including, of course, the HAP materials [6–10]. Several reinforcements are used to enhance the properties of HAP such as TiO_2, Al_2O_3, MgO or ZrO_2 [11–15]. Among these various additives zirconia (ZrO_2), which is a bioinert material, has been commonly used as reinforcement for many ceramics because of its high strength and fracture toughness. On the other hand, at high temperature (T > 1200 °C) HAP decomposes

to other CaP compounds, like α/β-TCP (tricalcium phosphate) or TTCP (tetracalcium phosphate). Besides, β-TCP has osteoconductive properties to be used as a coating for Ti implants, and many studies demonstrated its greater ability to form new bone after being implanted in the body [16–18].

ZrO_2 is an oxide which presents three types of crystalline structures at ambient pressure as follow: the monoclinic phase (*m*-ZrO_2), which is stable from room temperature up to 1170 °C and exhibits poor mechanical properties, the tetragonal phase (*t*-ZrO_2), which is stable in the temperature range 1170–2370 °C and has good mechanical properties, and the cubic phase (*c*-ZrO_2), which is stable above 2370 °C and has moderate mechanical properties [19–21]. It is known that the spontaneous transformation from the *t*-ZrO_2 to the more stable *m*-ZrO_2 is associated with a noticeable volume increase of the crystals. By mixing ZrO_2 with other metallic oxides, such as Y_2O_3 , MgO or CaO, great molecular stability can be achieved. Beside YSZ (yttrium–stabilized zirconia), which is the most studied combination [22], MgO present interesting properties in stabilization of zirconia. Magnesium stabilized zirconia has several advantages and can be developed with a good combination of mechanical and tribological properties by using the appropriate preparation technique [23]. Besides, MgO is an ample, low-cost, and mild antibacterial material, being safe for human beings [24–27].

To combine advantageous properties of HAP and ZrO_2 biomaterials one approach could be the preparation of composites [28]. Moreover, ZrO_2-HAP composites are considered to be interesting materials, due to the combination between two bioceramics, the inert ZrO_2 and the active HAP, which could increase the bonding ability with natural bone in many medical fields. Consequently, in the last years, many ZrO_2-HAP composites have been developed as coating or substrate in order to achieve both bone reconstruction and regeneration needed in the treatment of large bone defects [29].

The Co-Cr and Ni-Cr alloys are largely applied in dental restorations for repair prosthetic treatments, such as inlays, crowns, and fixed partial denture frameworks [30]. Despite certain disadvantages affecting their biocompatibility (such as local reactions of inflammation of surrounding tissue or systemic reactions (e.g., allergic reactions), the use of metallic alloys is due to their excellent mechanical properties and corrosion resistance, when in contact to a wet environment, containing various types of ions, pH changes, and mechanical or electrochemical wear. Although a huge variety of new polymeric or composite materials invaded the dental materials market, a detailed study on the metallic alloys as a skeleton for different zirconia-based ceramics is important and very interesting from a statistical point of view on the impact of using such kind of metallic-ceramics materials on the population health in a certain geographical region dependent on a unique dental materials market [31]. The oral rehabilitation purpose is to achieve better social integration and increased self-esteem and consist in the restoration of the patient's function and aesthetics. For achieving this goal saliva plays an essential role due to its numerous consequences, such as increased susceptibility to dental caries, periodontal tissue disease, dysgeusia, halitosis, and an increased incidence of oral infections. Also, the ingestion of certain foods can cause salivary pH changes from a neutral value to an acidic one, due to fermentation of carbohydrates by bacteria, bulimia, and gastroesophageal reflux disease. In this context, the study of pH influence on the behavior of either polymeric or metallic components of the oral restoration is important for an adequate choice of the treatment procedure [32].

This study aimed to prepare ZrO_2-based biocomposites by using different amounts of the bioinert ZrO_2, antibacterial MgO, and bioactive and biocompatible HAP, by ceramic method followed by sintering at high temperature. The obtained materials were further structural and morphological analyzed by X-ray powder diffraction (XRPD) and scanning electron microscopy/energy dispersive X-ray spectroscopy (SEM/EDS). Moreover, due to the fact that the composites could be used as protective coatings in the biomedical field, electrochemical impedance spectroscopy (EIS) measurements were carried out to evaluate

the anticorrosive properties of the prepared composites by in vitro preliminary tests, after immersion in artificial saliva of different pHs.

2. Materials and Methods

2.1. Reagents and Materials

The following reagents were used for HAP and ZrO_2-based composites preparations: calcium nitrate tetrahydrate (Merck, Germany), diammonium hydrogen phosphate (Merck, Germany), ammonia (25% solution, Posch Basic, Poland), ZrO_2 (Riedel-de Haën AG, Seelze, Germany, 99%), MgO (Alfa Aesar, Germany, 99.99%), HAP powders and PVA (polyvinyl alcohol 98-99% hydrolyzed, high molecular weight, Alfa Aesar, Germany).

HAP was prepared by the precipitation method previously described [33–35]. Briefly, the diammonium hydrogen phosphate (0.09 mol L^{-1}) and the ammonium 25% solution were slowly added to the calcium nitrate solution (0.15 mol L^{-1}). The pH of the reaction mixture was adjusted with ammonia solution to 11, and the reaction temperature was maintained at room temperature. The reaction mixture was stirred for 22 h. The Ca/P mole ratio was maintained at 1.67. After the reaction was accomplished, the precipitate was washed with ethanol and filtered. The filtered material was dried at 90 °C for 6 h.

ZrO_2-based composites were obtained by ceramic processing route [36]. The nominal compositions of the five prepared samples are presented in Table 1. The starting precursor powders were intimately grounded using an agate mortar and pestle. The resulted powders were mixed with 5% PVA and uniaxially cold pressed in a metallic dye into cylindrical pellets of 1 g with 10 mm in diameter at a pressure of 400 kgf using a Carver Inc. hydraulic press (Carver Inc, Wabash, IN, USA). Further, the pellets were sintered at 1600 °C using a Nabertherm LHT 04/16 furnace, under an air atmosphere with a heating and cooling rate of 5 °C/min and dwell time of 12 h at the maximum temperature. Afterward, all the prepared pellets were ground again to prepare the samples for XRPD, SEM/EDS, and electrochemical investigations.

Table 1. The nominal composition (wt.%) and notation of the samples.

Sample ID	ZrO_2 (wt.%)	MgO (wt.%)	HAP (wt.%)
S1	98.30	1.70	-
S2	93.39	1.61	5
S3	88.47	1.53	10
S4	68.81	1.19	30
S5	49.15	0.85	50

Due to the fact that the natural saliva is a complex matrix containing a great variety of compounds, and having changeable and unstable properties (during the day time or in the function of pH of food consumed), an artificial saliva which reproduced it, is actually impossible to obtain. Artificial saliva was prepared using the Mondelli receipt [37] containing appropriate quantities of the following salts purchased from Sigma Aldrich or "Reactivul" Bucuresti: NaCl (0.5 g/L), KCl (0.5 g/L), $CaCl_2 * 2H_2O$ (0.795 g/L), citric acide (0.0005 g/L), $NaH_2PO_4 * H_2O$ (0.78 g/L), urea (1 g/L), $(NH_4)_2SO_4$ (0.3 g/L) and $NaHCO_3$ (0.1 g/L). A diluted solution of H_3PO_4 (Sigma Aldrich) was used for pH adjustment to the desired value.

Two dental metallic alloys were purchased by MESA di Sala Giacomo & C S.n. c. having a composition declared by producer: Ni–Cr (Ni 63%, Cr 25%, Mo 10%, Si 1.5%, others Mn, Al, Zr, Ce, La) and Co–Cr (Co 65%, Cr 29%, Mo 5%, C 0.4%, Si 0.35%, Mn 0.25%). The chitosan solution was obtained by dissolving 10 mg chitosan (from Sigma Aldrich, from crab shells) to 10 mL of 0.1 M acetic acid, followed by a sonication step, for 30 min.

Distilled water was used for preparing all solutions. All reagents having p.a. quality, were used without supplementary purification.

2.2. Preparation of the Composite based Modified Ni-Cr or Co-Cr Electrodes

The dental metallic alloys samples have a cylindrical form and were embedded into a Teflon holder, such that a 3 mm diameter circle surface could be investigated. Before using, the surface of the dental Ni-Cr or Co-Cr alloys electrode was thoroughly polished on alumina slurry (of successively gradations: 500, 1000 and 4000). In order to remove alumina particles and other possible contaminants, the electrodes were sonicated for 5 min in acetone, then well-rinsed with distilled water and dried.

The ZrO_2 and S1–S5 composites were immobilized onto metals alloy electrode surfaces by using a chitosan membrane. Thus, 1 mg of ZrO_2 or S1–S5 composites were dispersed in 1 ml of chitosan solution, and the suspension was sonicated for 2 h. The drop-casting method of immobilisation consists in the deposition of 5 µL of the obtained suspension onto the clean alloy electrode surface and kept for drying under a beaker during 2 h, at room temperature.

2.3. Investigation Methods

The prepared composites were morpho-structurally analyzed. Structural analyses were performed on S1–S5 composites using a Shimadzu XRD-6000 diffractometer operating at 40 kV, 30 mA with a monochromator of graphite for CuKα (λ = 1.54060 Å). The diffraction patterns were recorded in the 2θ range of 10–80 at a scan speed of 2 °/min. Scanning Electron Microscopy (SEM) analysis was performed using a Hitachi SU8230 (Tokyo, Japan) microscope. The electron microscope was coupled with an Aztec X-Max 1160 energy dispersive X-ray (EDX) detector (Oxford Instruments).

The electrochemical measurements were performed by using a PC controlled electrochemical analyser (AUTOLAB PGSTAT302NEcoChemie, Utrecht, Netherlands) controlled by GPES 4.7 software for cyclic voltammetry and open circuit potential measurements, and FRA 2.1 software for impedance measurements. An undivided three-electrodes cell was connected to the potentiostat and was equipped with the prepared modified alloys electrodes, i.e. Co-Cr/Chit-ZrO_2, Co-Cr/Chit-Sx (where x = 1÷5) or Ni-Cr/Chit-ZrO_2, Ni-Cr/Chit-Sx (where x = 1÷5), as working electrode, a Pt wire, as counter electrode, and a Ag/AgCl, KCl_{sat} as reference electrode. The open circuit potential (OCP) was recorded during 3600 s. The corrosion tests were carried out after the stabilization of unmodified and modified electrodes, under open circuit conditions.

Impedance spectra at unmodified and modified dental Ni–Cr and Co–Cr alloys interface were recorded at the OCP value, by using an AC signal with amplitude of ±10 mV and a frequency range from 100 kHz down to 0.1 Hz. Electrochemical impedance spectroscopy (EIS) data were plotted as Nyquist and Bode diagrams. The experimental impedance data were fitted by using an equivalent electric circuit and a ZSimpWin 3.21 software. The parameters values of the electric circuit components were subsequently correlated with the processes occurring at the modified electrode surface. The electrode investigations were carried out at three pH values, namely: pH 6 (simulating a normal body environment), pH 5 and pH 4.3 (digestion situation) [38].

The pH of the artificial saliva was adjusted using a glass combined electrode (HI 11310) connected to a pH-meter (type MV 870, Pracitronic, Germany), by addition of small volumes of diluted H_3PO_4. All experiments were performed in aerated solutions at ambient temperature and repeated three times, using for each experiment a new modified surface of metallic alloy electrode.

3. Results and Discussion

3.1. Morpho-Structural Characterization of Composites

In order to evaluate the structural properties of the prepared composites, XRPD analysis was performed. Figure 1 displays the XRPD patterns of the prepared composites, after sintering in the air at 1600 °C.

Analysis of powder pattern of the S1–S5 samples showed peaks which correspond to both *t*-ZrO_2 and *m*-ZrO_2 phases in different ratios. No peaks belonging to the MgO

phases were observed at this Mg doping level, confirming the solubility of Mg in the ZrO_2. Besides, small peaks which could be assigned to β-TCP phase were identified. However, no characteristic peaks corresponding to any other CaP-compounds, like HAP, TTCP (tetracalcium phosphate), $CaZrO_3$ or CaO were detected for S2–S5 samples. It is known that these crystal structure transformations are the reactions that generally occur when sintering ZrO_2 and HAP at a high temperature. At higher sintering temperatures (T > 1200 °C), HAP decomposed in the presence of ZrO_2 as follows [39]:

$$Ca_{10}(PO_4)_6(OH)_2 + ZrO_2 \rightarrow 3Ca_3(PO_4)_2 + CaZrO_3 + H_2O \quad (1)$$

where HAP decomposes into α/β -TCP with the appearance of the second phase of $CaZrO_3$. The decomposition rate of HAP to α/β -TCP is improved with increasing the ZrO_2 concentration in the samples, zirconia works as a catalyst [39].

Lukič et al. have synthesized HAP nano powder in the presence of zirconium (Zr^{4+}) ions and they reported that the phase transformations could be tailored by adjusting zirconium content [40]. They showed that the complete phase transformation from HAP to β-TCP provoked stress-induced transformation of *t*-ZrO_2 to *m*-ZrO_2. In our case, taking into account that the ZrO_2/MgO mole ratio was maintained the same in the preparation of the composites, the zirconia phase transformation may be due to the HAP decomposition.

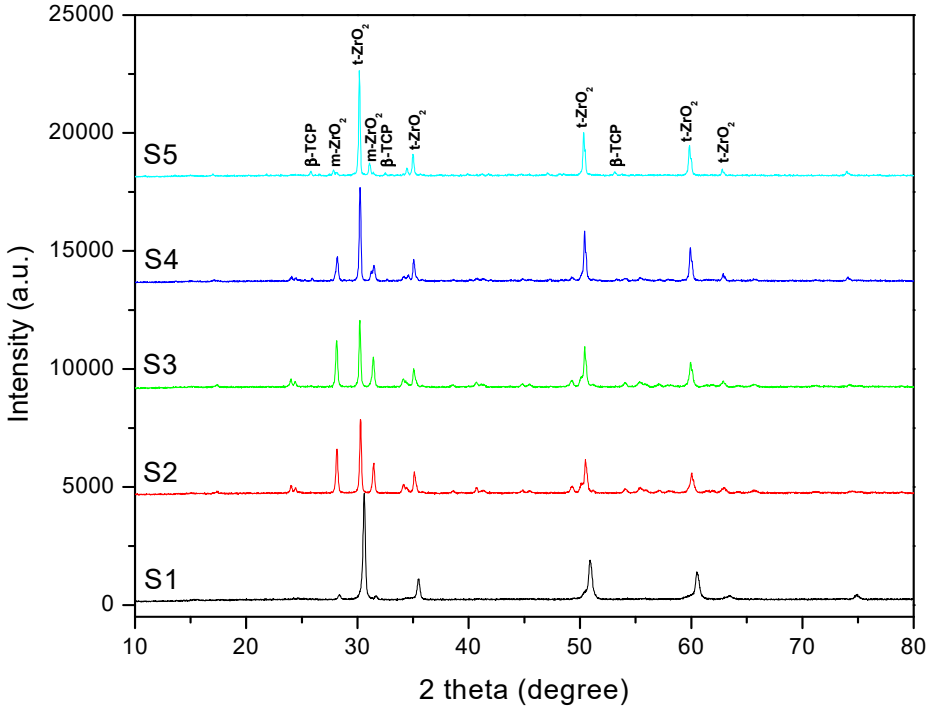

Figure 1. XRPD patterns of the prepared composites.

The crystallite sizes (D) of the composites were calculated based upon on the (101) diffraction peak's broadening in the XRD pattern using the Scherrer equation:

$$D_{hkl} = 0.9\lambda/(\beta\cos\theta) \quad (2)$$

where: D- crystallite size along (hkl) direction, β- full width half maximum (FWHM) of the most intense diffraction line, λ- wavelength of X-ray, θ- the Bragg angle [41]. The crystallite sizes estimated using the Scherrer equation are ranged in the nanometric domain, with values from 37.98 nm to 60.64 nm, for both *m*- and *t*-ZrO_2 phases.

SEM/EDS analyses were performed for morphological characterization and to detect chemical elemental composition on the surface of the S2–S5 composites. The surface morphology appears homogenous and consists of small grains (30–50 μm) as shown in

Figure 2. Pores are also observed for all the studied composites. The results of EDS analysis corresponding to the same nominal cationic compositions highlight the simultaneous presence of the Zr, Mg, Ca, and P elements, and no others were systematically detected. Moreover, for the S5 composite, where XRPD analysis detected the presence of β-TCP as a secondary phase, a Ca/P mole ratio of 1.55 was found, which is close to the theoretical Ca/P mole ratio in β-TCP.

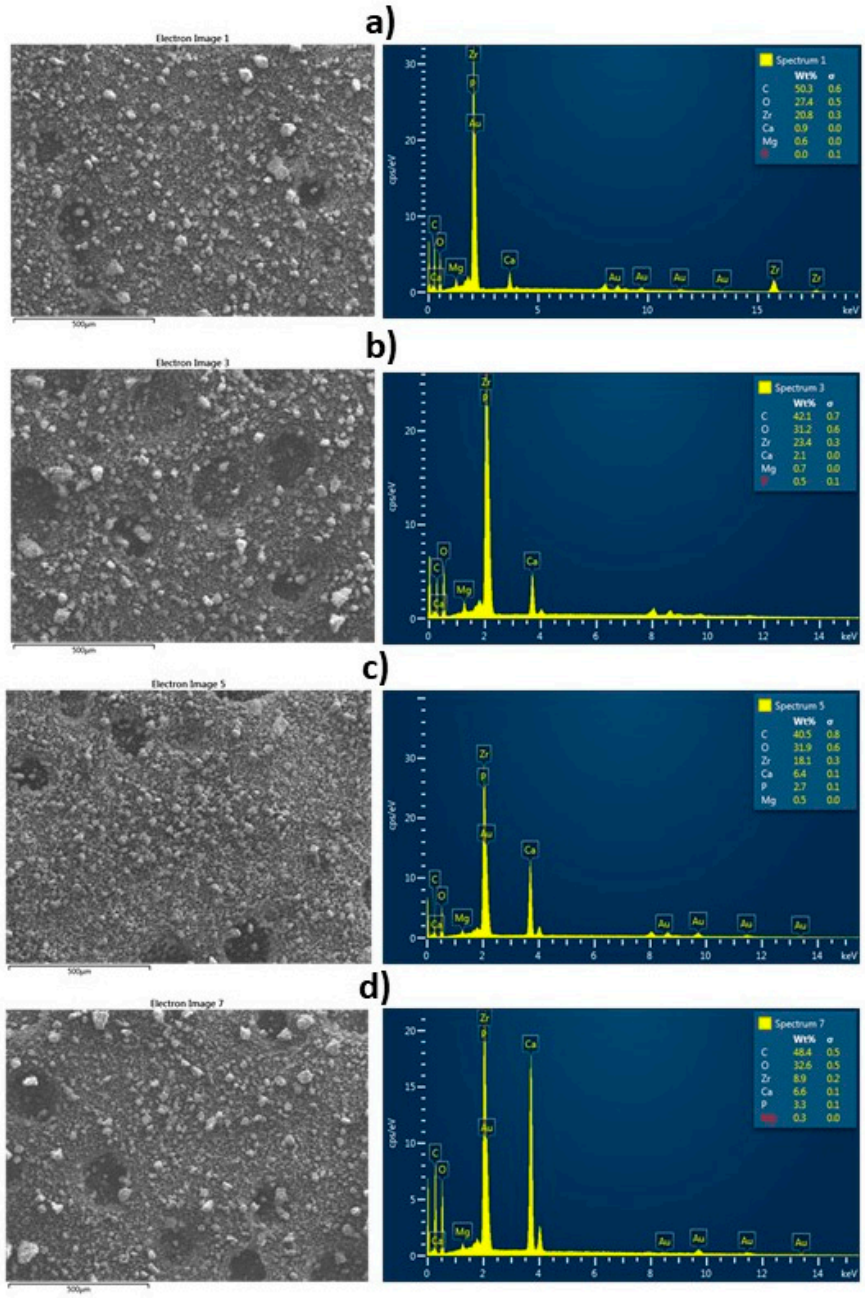

Figure 2. SEM images (left) and EDS analysis (right) for S2 (**a**), S3 (**b**), S4 (**c**) and S5 (**d**) composites.

3.2. Electrochemical Behaviour of Metallic Alloys by Cyclic Voltammetry

3.2.1. The Potential in Open Circuit (OCP)

The value of the potential in open circuit (OCP) is an indicator of the anticorrosive tendency of metal and has an irreversible character because the instability of the metal-solution interface. The OCP dependence on time exhibited that the potentials of all the studied electrode materials are on an ascending trend in the first part of the recording

period (approx. first 35 min), after that they reaching the equilibrium values (results not shown). Consequently, due to the fact that the active surface is very small (0.0707 cm^2), an interval time period of 3600 s for obtaining the constant OCP values is considered to be optimal for reaching a quasi-equilibrium state at the electrode/solution interface [42]. The OCP stabilized values for all electrodes in all studied pH values are summarized in Figure 3. As shown in the literature the anti-corrosion performance of a coating/metal system is generally predictable, if the OCP of coated metal is more positive than that of the bare metal [43].

This is confirmed by analyzing the results of Figure 3, where it can be observed that the OCP values at the bare surface are the smallest and the OCP values are spread on an approximatively 200 mV range. Also, it can be observed, in all cases and all pH values, the same tendency of increasing/decreasing of the OCP values during the exposure of the samples to artificial saliva, irrespective of metallic alloy supports. This behavior is usually be attributed to thickening of the passive film, which becomes more protective conferring to the alloy more anticorrosive properties [44]. Also, it can be observed that the presence of composite layer on the metallic dental alloy surface, increases the OCP values for the majority of cases, proving its complementary protective properties in acidic pH values of artificial saliva (i.e., 4.3 and 5).

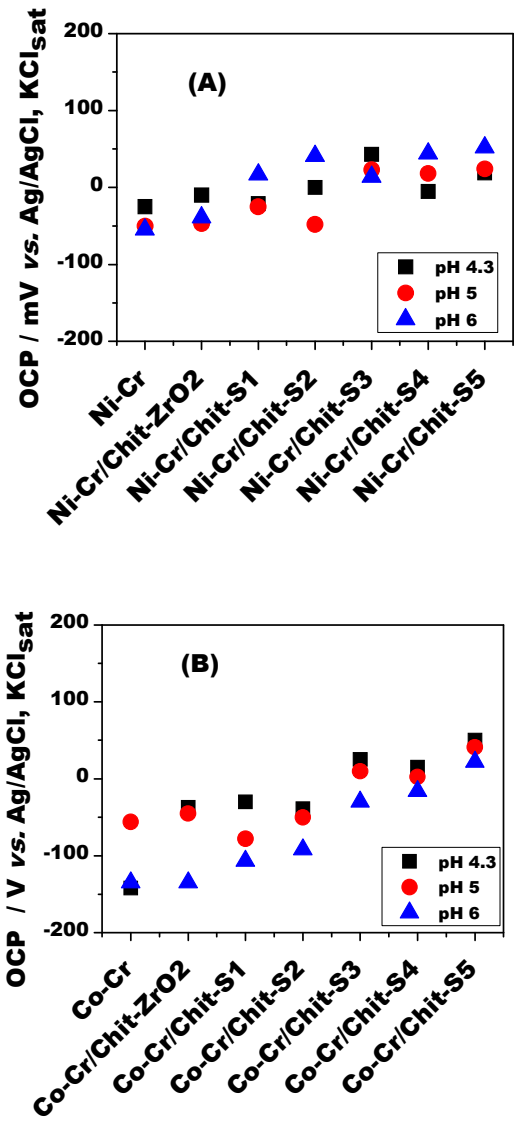

Figure 3. Variation of open circuit potential at Ni-Cr (**A**) and Co-Cr (**B**) based modified electrodes and at different pH values.

In order to establish if a dental alloy will suffer corrosion under certain condition of the oral cavity, the OCP value determination is necessary, but not sufficient, because OCP is a thermodynamic measure which gives only information related to the Gibbs free energy of the electrochemical system [31,45].

3.2.2. EIS Measurements

Electrochemical impedance spectroscopy (EIS) is an *ac* complex technique used to evaluate the electrical behavior of a material, by modelling the real system in terms of an equivalent circuit containing resistive, capacitive and diffusive components.

In order to obtain further information on the corrosion resistance properties of the both studied metallic dental alloys surfaces unmodified and modified with a layer of ZrO_2 or Sx (where x = 1÷5) composite in chitosan, impedance measurements were recorded with the electrodes immersed in artificial saliva of pH 4.3, 5 and 6, after 3600 s for OCP stabilization.

The obtained impedance spectrum was fitted by using a non-linear regression method, and the values of the obtained parameters of two used equivalent circuit models (i.e., $R_s(Q_{dl}R_{ct})$, $R_s(Q_{layer}R_{layer})(Q_{dl}R_{ct})$) (Figure 4) were summarized in Tables 2 and 3 for all studied composite matrix/dental alloys interfaces and all pH, respectively. The significance of the components of the equivalent circuits is as following: R is the resistance corresponding to the uncompensated solution (R_s), to the composite matrix (R_{layer}) and to the charge transfer process (R_{ct}) respectively; Q is the constant phase element corresponding to the composite matrix (Q_{layer}) or double layer (Q_{dl}), respectively.

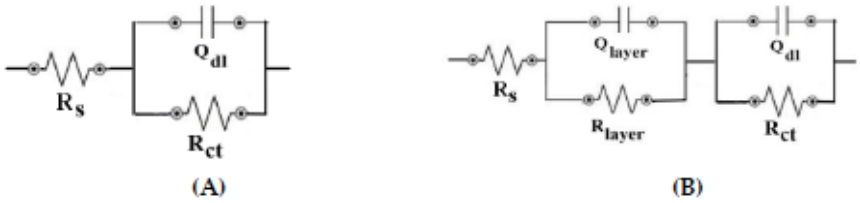

Figure 4. Equivalent electric circuits $R_s(Q_{dl}R_{ct})$ (**A**) and $R_s(Q_{layer}R_{layer})(Q_{dl}R_{ct})$ (**B**) used for fitting experimental data.

As known, R_{ct} is a quantitative parameter, which could be an indicator of corrosion resistance of the composite thin film acting as a barrier to electron flow (resistor) and provides a value of the degree of protection furnished by the composite thin film deposited on the metallic dental alloy interface [46,47].

Due to lack of surface homogeneity of surface polishing, the presence of the composite matrix coating and the distortions on the double-layer, the constant phase element (Q) instead of an "ideal" capacitor was incorporated into the equivalent circuit models, in order to appropriately fit the experimental data. The equivalent capacitance of the Q was modelled as a non-ideal capacitor containing the capacitance of the double layer C_{dl} and a roughness factor n, using the formula $Q = (C_{dl}\ R_{ct})^{1/n}/R_{ct}$ [48]. The roughness factor n is a number placed in the range 0–1, and it gives information about surface roughness (i.e., n = 1 is the case of a perfectly smooth surface of an ideal capacitor, and n = 0 is the case of an ideal resistance, respectively) [46,47].

From the data presented in Tables 2 and 3 it can be observed that R_s value doesn't changed considerably during the experiment, having values in the range of 15–60 ohm$\times$cm^2, because the factors affecting its value like the stability of exposed surface and ions concentration in artificial saliva solution doesn't changed dramatically in the studied pH range. When a charge transfer reaction occurring to a metallic surface can be neglected as in the case of corrosion process, the corresponding estimated impedance could be attributed to the impedance of inorganic/organic composite protective coatings [31,49]. In Figure 5A–F, the Nyquist plots exhibit a depressed, capacitive-like semicircle and a second linear region, one at high frequencies and another at intermediate and lower frequency values, respec-

tively, for all studied interfaces. This behavior is due to the inorganic/organic composite protective coatings having corrosion protection properties.

Table 2. Electrochemical impedance spectroscopy data of Ni-Cr, Ni-Cr/Chit-ZrO_2 and Ni-Cr/Chit-Sx (where x = 1-5) after immersion in artificial saliva of different pH values, using $R_s(Q_{dl}R_ct)$ or $R_s(Q_{layer}R_{layer})(Q_{dl}R_{ct})$ equivalent electric circuit.

	R_s [ohm×cm^2]	Q_{layer} [S×s^n/cm^2]	n_1	R_{layer} [ohm×cm^2]	Q_{dl} [S×s^n/cm^2]	n_2	R_{ct} [ohm×cm^2]	Chi^2
				pH 4.3, Ni-Cr				
Ni-Cr	55.88 ± 0.45	5.90×10^{-5} ± 0.48	0.715	-	-	-	59.86×10^3 ± 2.49	1.5×10^{-3}
Ni-Cr/Chit-ZrO_2	17.22 ± 0.40	23.94×10^{-5} ± 9.60	0.708	37.46 ± 5.95	7.57×10^{-5} ± 0.44	0.826	104.90×10^3 ± 4.68	0.09×10^{-3}
Ni-Cr/Chit-S1	22.93 ± 4.43	21.68×10^{-5} ± 2.7	0.540	27.24 ± 7.33	12.65×10^{-5} ± 3.6	0.730	128.63×10^3 ± 1.82	5.5×10^{-3}
Ni-Cr/Chit-S2	28.71 ± 0.73	7.69×10^{-5} ± 0.65	0.789	104.50 ± 6.18	16.07×10^{-5} ± 9.37	0.616	153.29×10^3 ± 10.45	0.16×10^{-3}
Ni-Cr/Chit-S3	26.16 ± 0.49	19.59×10^{-5} ± 10.18	0.702	78.79 ± 9.42	8.07×10^{-5} ± 0.66	0.779	103.59×10^3 ± 7.58	0.15×10^{-3}
Ni-Cr/Chit-S4	24.6 ± 0.71	25.54 × 10−5 ± 1.82	0.679	47.98 ± 10.03	8.18×10^{-5} ± 0.422	0.792	185.50×10^3 ± 2.67	0.27×10^{-3}
Ni-Cr/Chit-S5	20.43 ± 0.38	8.63×10^{-5} ± 0.44	0.779	69.79 ± 5.67	20.74×10^{-5} ± 6.77	0.682	136.7×10^3 ± 7.16	0.07×10^{-3}
				pH 5, Ni-Cr				
Ni-Cr	45.66 ± 0.71	7.86×10^{-5} ± 0.66	0.661	-	-	-	46.50×10^3 ± 3.54	2.5×10^{-3}
Ni-Cr/Chit-ZrO_2	18.16 ± 0.458	50.41×10^{-5} ± 10.86	0.600	31.76 ± 6.28	7.40×10^{-5} ± 0.36	0.834	76.10×10^3 ± 2.79	0.07×10^{-3}
Ni-Cr/Chit-S1	22.97 ± 2.7	10.48×10^{-5} ± 2.3	0.672	20.70 ± 6.19	16.5×10^{-5} ± 2.35	0.580	147.69×10^3 ± 1.21	1.8×10^{-3}
Ni-Cr/Chit-S2	17.38 ± 0.814	8.08×10^{-5} ± 0.69	0.764	57.53×10^3 ± 4.26	21.25×10^{-5} ± 13.14	0.629	148.9×10^3 ± 7.56	0.16×10^{-3}
Ni-Cr/Chit-S3	19.61 ± 0.43	15.49×10^{-5} ± 6.85	0.714	89.7 ± 6.36	7.57×10^{-5} ± 0.54	0.791	225.90×10^3 ± 1.26	0.11×10^{-3}
Ni-Cr/Chit-S4	19.18 ± 0.92	21.75×10^{-5} ± 2.11	0.668	41.06 ± 9.95	8.84×10^{-5} ± 0.51	0.771	169.5×10^3 ± 3.27	0.38×10^{-3}
Ni-Cr/Chit-S5	15.59 ± 0.45	34.57×10^{-5} ± 9.02	0.672	52.07 ± 10.58	8.65×10^{-5} ± 0.73	0.789	108.1×10^3 ± 1.19	0.09×10^{-3}
				pH 6, Ni-Cr				
Ni-Cr	23.09 ± 0.59	7.98×10^{-5} ± 1.18	0.823	-	-	-	69.7×10^3 ± 9.40	1.2×10^{-3}
Ni-Cr/Chit-ZrO_2	23.14 ± 0.32	6.79×10^{-5} ± 0.34	0.828	51.72 ± 5.5	31.12×10^{-5} ± 7.3	0.657	76.3×10^3 ± 2.40	0.06×10^{-3}
Ni-Cr/Chit-S1	40.09 ± 7.8	4.11×10^{-5} ± 0.31	0.727	11.31 ± 3.2	3.36×10^{-5} ± 9.5	0.700	137.5×10^3 ± 2.36	5.3×10^{-5}
Ni-Cr/Chit-S2	48.62 ± 0.64	8.56×10^{-5} ± 0.56	0.777	76.1 ± 6.15	22.24×10^{-5} ± 1.32	0.575	84.7×10^3 ± 5.34	0.10×10^{-3}
Ni-Cr/Chit-S3	39.98 ± 0.48	7.50×10^{-5} ± 0.53	0.814	70.1 ± 10.5	39.35×10^{-5} ± 1.27	0.612	138.0×10^3 ± 7.66	0.11×10^{-3}
Ni-Cr/Chit-S4	35.66 ± 0.735	8.01×10^{-5} ± 0.65	0.799	43.65 ± 1.27	45.92×10^{-5} ± 2.19	0.583	92.9×10^3 ± 6.56	0.17×10^{-3}
Ni-Cr/Chit-S5	33.44 ± 0.46	48.49×10^{-5} ± 9.69	0.588	77.58 ± 10.46	7.85×10^{-5} ± 0.82	0.852	112.9×10^3 ± 1.51	0.09×10^{-3}

Values ± relative standard errors (RSD) expressed in percent (%).

Table 3. Electrochemical impedance spectroscopy data of Co-Cr,Co-Cr/Chit-ZrO_2 and Co-Cr/Chit-Sx (where x = 1-5) after immersion in artificial saliva of different pH values, using $R_s(Q_{dl}R_ct)$ or $R_s(Q_{layer}R_{layer})(Q_{dl}R_{ct})$ equivalent electric circuit.

	Rs [ohm×cm²]	**Q_{layer} [S×sⁿ/cm²]**	**n_1**	**R_{layer} [ohm×cm²]**	**Q_{dl} [S×sⁿ/cm²]**	**n_2**	**R_{ct} [ohm×cm²]**	**Chi²**
				pH 4.3, Co-Cr				
Co-Cr	30.21 ± 3.17	9.61×10^{-5} ± 2.39	0.729	-	-	-	29.06×10^3± 7.04	7.8×10^{-3}
Co-Cr/Chit-ZrO_2	16.91 ± 0.66	5.89×10^{-5} ± 2.66	0.918	46.69×10^3 ± 2.64	5.70×10^{-5}± 4.14	0.877	68.4×10^3± 7.4	0.4×10^{-3}
Co-Cr/Chit-S1	34.82 ± 2.6	12.6×10^{-5} ± 4.6	0.693	224.8×10^3 ± 2.28	9.27×10^{-5}± 7.8	0.897	136.4×10^3± 1.78	3.3×10^{-3}
Co-Cr/Chit-S2	28.92 ± 1.00	13.72×10^{-5} ± 1.44	0.637	87.1 ± 6.47	7.88×10^{-5}± 0.48	0.777	192.6×10^3± 3.15	0.93×10^{-3}
Co-Cr/Chit-S3	25.07 ± 0.58	4.25×10^{-5} ± 8.32	0.815	75.64×10^3 ± 10.68	12.78×10^{-5}± 1.99	0.945	329.7×10^3± 1.94	0.38×10^{-3}
Co-Cr/Chit-S4	23.17 ± 0.58	4.34×10^{-5} ± 1.27	0.862	22.37×10^3 ± 6.47	16.47×10^{-5}± 5.42	0.766	163.1×10^3± 9.66	0.34×10^{-3}
Co-Cr/Chit-S5	23.36 ± 0.58	4.49×10^{-5} ± 4.31	0.825	17.61×10^3 ± 11.45	20.08×10^{-5}± 1.64	0.811	151.6×10^3± 3.28	0.41×10^{-3}
				pH 5, Co-Cr				
Co-Cr	35.75 ± 3.35	6.09×10^{-5} ± 2.42	0.760	-	-	-	12.24×10^3 ± 8.36	9.1×10^{-3}
Co-Cr/Chit-ZrO_2	19.98 ± 0.51	8.18×10^{-5} ± 4.23	0.870	7.43×10^3 ± 6.92	4.88×10^{-5} ± 1.71	0.914	88.14×10^3 ± 1.68	0.2×10^{-3}
Co-Cr/Chit-S1	24.83 ± 2.65	11.61×10^{-5} ± 6.33	0.834	5.11×10^3 ± 2.44	11.47×10^{-5} ± 6.5	0.698	164.2×10^3 ± 1.48	2.4×10^{-3}
Co-Cr/Chit-S2	18.44 ± 1.11	46.52×10^{-5} ± 2.20	0.980	5.18×10^3 ± 1.77	5.36×10^{-5} ± 2.40	0.717	120.2×10^3 ± 8.06	1.79×10^{-3}
Co-Cr/Chit-S3	16.98 ± 0.84	5.02×10^{-5} ± 2.69	0.789	11.22×10^3 ± 10.65	16.89×10^{-5} ± 9.06	0.749	356.5×10^3 ± 3.51	0.53×10^{-3}
Co-Cr/Chit-S4	17.66 ± 0.87	4.85×10^{-5} ± 10.49	0.829	12.09×10^3 ± 2.67	17.18×10^{-5} ± 2.89	0.829	188.44×10^3 ± 3.63	0.87×10^{-3}
Co-Cr/Chit-S5	16.03 ± 0.96	6.61×10^{-5} ± 3.96	0.843	19.76×10^3 ± 7.48	7.20×10^{-5} ± 3.5	0.854	**434.2×10^3 ± 3.55**	1.14×10^{-3}
				pH 6, Co-Cr				
Co-Cr	22.65 ± 1.87	8.645×10^{-5} ± 1.33	0.805	-	-	-	18.9×10^3 ± 8.14	3.4×10^{-3}
Co-Cr/Chit-ZrO_2	22.25 ±0.53	3.93×10^{-5} ±6.33	0.943	124.4×10^3 ± 10.87	9.52×10^{-5} ± 2.5	0.838	67.9×10^3 ± 3.42	0.3×10^{-3}
Co-Cr/Chit-S1	33.16 ±1.38	7.04×10^{-5} ±8.02	0.803	4.97×10^3 ± 3.13	7.97×10^{-5} ± 8.1	0.772	143.2×10^3 ± 9.35	1.0×10^{-3}
Co-Cr/Chit-S2	32.25 ± 0.82	6.31×10^{-5} ± 3.36	0.926	14.64×10^3 ± 9.66	10×10^{-5} ± 5.73	0.684	120.5×10^3 ± 8.29	0.65×10^{-3}
Co-Cr/Chit-S3	61.21 ± 0.52	19.13×10^{-5} ± 5.52	0.752	148.5×10^3 ± 10.43	4.23×10^{-5} ± 1.26	0.858	112.8×10^3 ± 4.76	0.33×10^{-3}
Co-Cr/Chit-S4	29.28 ± 0.62	13.98×10^{-5} ± 4.17	0.859	171.3×10^3 ± 2.86	4.07×10^{-5} ± 1.41	0.857	135.78×10^3 ± 2.66	0.25×10^{-3}
Co-Cr/Chit-S5	34.50 ± 0.79	4.92×10^{-5} ± 7.43	0.851	19.45×10^3 ± 1.82	19.12×10^{-5} ± 2.53	0.832	180.02×10^3 ± 3.38	0.82×10^{-3}

Values ± relative standard errors (RSD) expressed in percent (%).

Analyzing the data from Tables 2 and 3, the following information could be observed. In the case of bare Ni-Cr or Co-Cr metallic alloys the charge transfer resistance is in the range of 12–70 kohm×cm^2, proving that the oxide passive layer is a weak protective against corrosion in artificial saliva of pH 4.3-6. Moreover, the Chit-ZrO_2 composite matrix on

both Ni-Cr and Co-Cr exhibit R_{ct} values higher than that obtained for bare electrode (in the range 70–90 kohm×cm^2), irrespective of studied pH values, proving the beneficial effect of this coating. For all Chit-Sx (x = 1÷5) composite matrix deposited on both Ni-Cr or Co-Cr metallic supports at all studied pHs, the values of R_{ct} are higher than those determinated at bare or Chit-ZrO_2 composite coating. Additionally, the R_{ct} values higher than 100 kohm×cm^2 which can rich 450 kohm×cm^2 (for particular electrode configuration or pH) indicate that Chit-Sx (x = 1÷5) composite matrix has anticorrosive protective properties. The behavior could be correlated with SEM/EDS experiments and could be attributed either to the quasi similar compact aspect of the composites S2–S5, or to the presence of increasing amount of Ca.

The highest R_{ct} values, which means the best protective properties of the coatings, are increasing in the following order: Ni-Cr/Chit-S3 (pH 6, 138 kohm×cm^2) < Ni-Cr/Chit-S4 (pH 4, 185.5 kohm×cm^2) < Ni-Cr/Chit-S3 (pH 5, 225 kohm×cm^2) or Co-Cr/Chit-S5 (pH 6, 180 kohm×cm^2) < Co-Cr/Chit-S3 (pH 4, 329.7 kohm×cm^2) < Co-Cr/Chit-S5 (pH 5, 434.2 kohm×cm^2).

It can be seen that the best resistance at corrosion shown the composites S3–S5 having an increased amount of Ca in their initial and final composition (see EDS results in Figure 2). Also, the small differences between the R_{ct} values of the composites S3–S5 could be due to the similar behavior concerning the electrolyte diffusion through the composite layer, without reaching the metallic surface [50].

A roughness factor n = 0.56 ÷ 0.95 in all studied cases indicates that an oxide passive film is formed on both metallic interfaces, suggesting a deviation of their behavior from pure ideal capacitor comportment. For all fitted data presented in Tables 2 and 3, the Chi-square distribution test (χ^2) have values between $10^{-2} \div 10^{-4}$, and the relative standard errors (RSD, expressed in %) are less than 20%, indicating excellent agreement between the experimental and fitted data, and proving the correct choice of electric elements in the equivalent circuit model [51].

In the corresponding Bode impedance plots (Figure 6A–F), in the case of Chit-S1 inorganic/organic matrix deposited on both metallic dental alloys, immersed in artificial saliva irrespective of pH values, the total |Z| impedance values is lower than for all other tested composite (i.e., Chit-Sx, where x = 2÷5). The same small total |Z| impedance value is observed in the case of Chit-S5 deposited on Ni-Cr metallic support and of Chit-ZrO_2 deposited on Co-Cr metallic support. This means that the presence of increased weight of Ca in the Chit-S5 composite matrix (on Ni-Cr) act similarly with pure ZrO_2 (Chit-ZrO_2 coating on Co-Cr) or ZrO_2-MgO (Chit-S1 coating on both Ni-Cr and Co-Cr) and its absence or presence in the coating matrix, in a certain weight, maybe prevent the Chit swelling or dissolution [52]. In a previously work [31], it was demonstrated that the roughness of the metallic Ni-Cr electrode surface is more significant than that of the Co-Cr metallic electrode surface, leading to a better immobilization of the composite layer. Moreover, this result indicates that there should be a minimum of Ca amount in the composite matrix from which the anticorrosive resistance of the protective layer become significant.

In the 0.1–10^5 Hz frequency range of the Bode diagrams (Figure 6A–F) it can be observed that the slope of the impedance diagram was around - 0.75 and the maximum phase angle values is between 60–80°, in the case of all Chit-Sx (where x = 2÷5) matrices containing HAP in the initial synthesis mixture. Exception are the cases of Chit-S1, Chit-S5 (at both pH 4.3, 5) and Chit-ZrO_2 (pH 6) on Ni-Cr, and Chit-S1 and Chit-ZrO_2 (all pHs) on Co-Cr metallic supports, respectively, where the slope of the impedance was around −0.35 in the same frequency range (i.e., 0.1–1000 Hz) and the phase angle was around 90° for frequencies greater than 10^3 Hz. This behavior suggests a possibly existence of a synergetic effect between the diffusion process through the Chit-composite layer and the roughness of the metallic surface of the electrode [31,50,52].

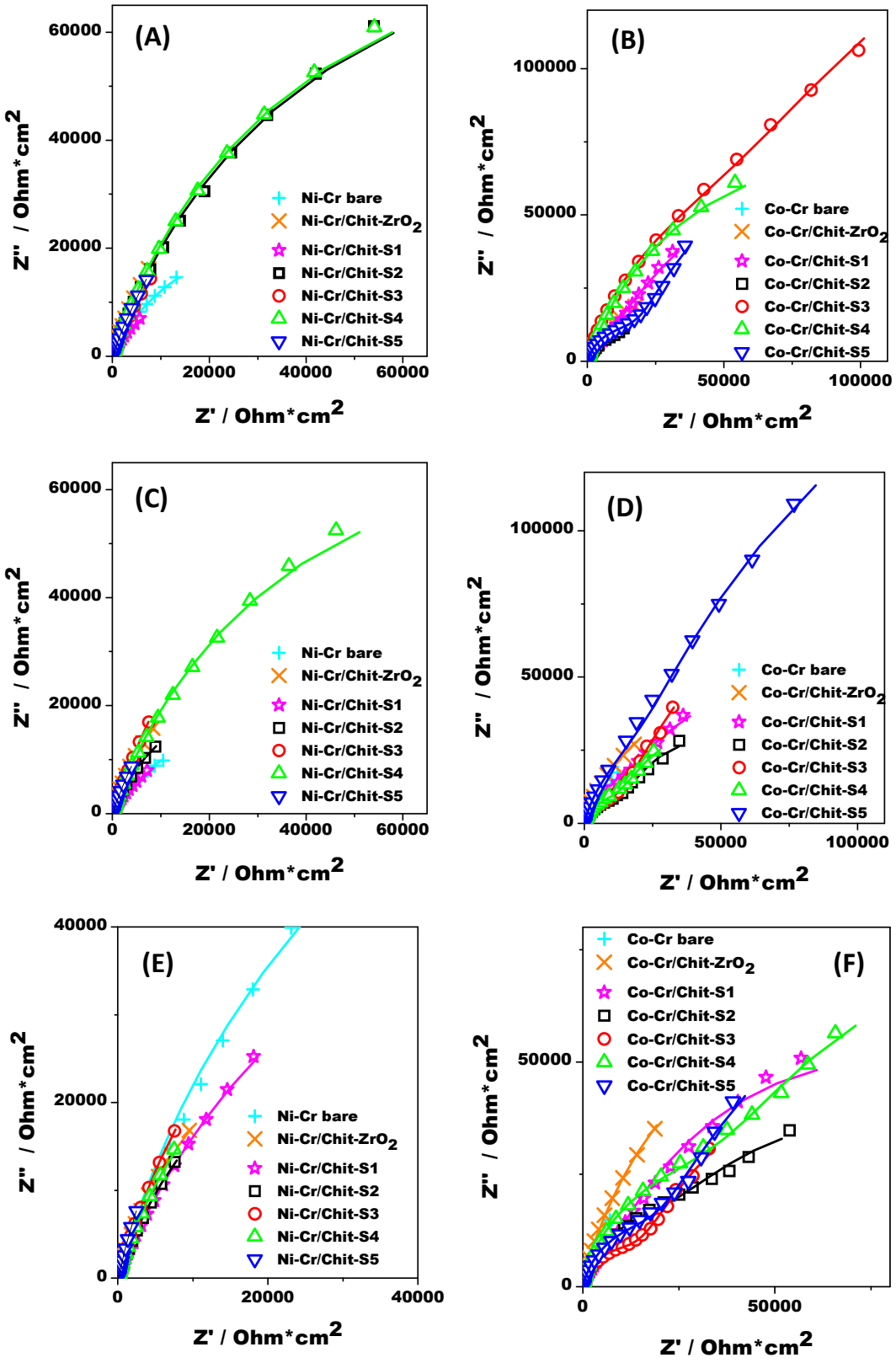

Figure 5. Nyquist impedance diagram for Ni-Cr (**A**,**C**,**E**) and Co-Cr (**B**,**D**,**F**) bare electrodes (+, cyan) and covered with ZrO_2 (X, orange), S1 (∗, magenta), S2 (□, black), S3 (○, red), S4 (△, green), S5 (▽, blue) in chitosan membrane, recorded at the open circuit potential in artificial saliva of pH 4.3 (**A**,**B**), pH 5 (**C**,**D**), pH 6 (**E**,**F**) and the corresponding simulated data (solid line).

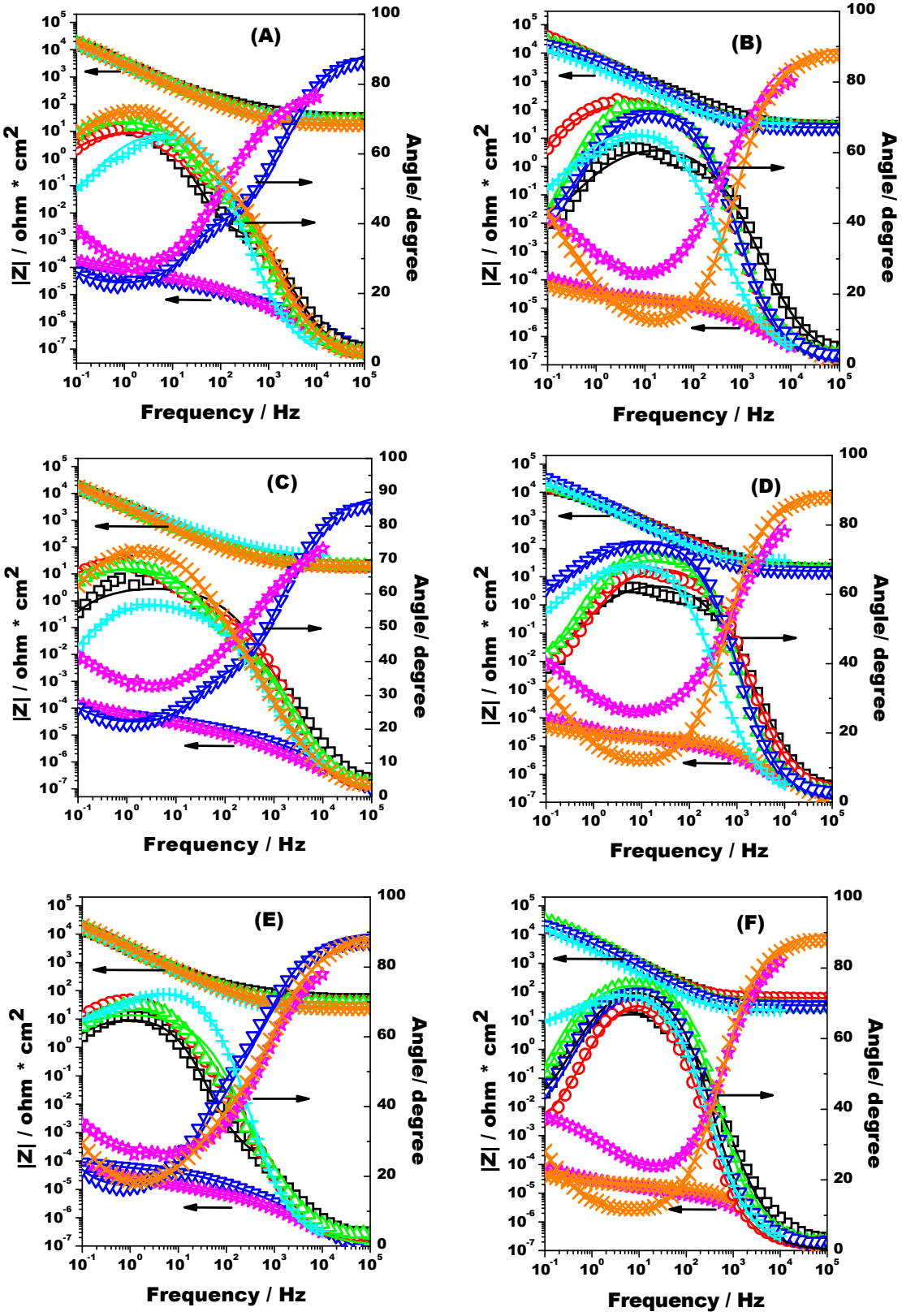

Figure 6. Bode diagram (log |Z| *vs*.log f and phase angle *vs*.log f) for measured data at Ni-Cr (**A**,**C**,**E**) and Co-Cr (**B**,**D**,**F**) bare electrodes (**+**, cyan) and covered with ZrO_2 (**X**, orange), S1 (∗, magenta), S2 (□, black), S3 (○, red), S4 (△, green), S5 (▽, blue) in chitosan membrane, recorded at the open circuit potential in artificial saliva of pH 4.3 (**A**,**B**), pH 5 (**C**,**D**), pH 6 (**E**,**F**) and the corresponding simulated data (solid line).

4. Conclusions

ZrO_2-based composites, based on different amounts of antibacterial magnesium oxide and bioactive and biocompatible hydroxyapatite to the inert zirconia, were prepared by ceramic method at high temperature, and morpho-structurally characterized by XRPD and SEM/EDS. Moreover, HAP decomposition at this high sintering temperature could play an important role in the anticorrosive properties if these composites are used as coating materials.

Two metallic dental alloys (i.e., Ni–Cr and Co–Cr) coated with a chitosan membrane containing the prepared composites were exposed to aerated artificial saliva solutions of different pHs (i.e., 4.3, 5, 6) and the corrosion resistance was investigated by electrochemical impedance spectroscopy technique. However, from the fitted data (using $R_s(Q_{dl}R_{ct})$ or $R_s(Q_{layer}R_{layer})(Q_{dl}R_{ct})$ electrical circuits) it was observed that the two investigated metallic dental alloys shown quasi-similar anticorrosive properties when coated with layers containing different ZrO_2-based composites, probably due to the synergetic effect between the diffusion process through the Chit-composite layer and the roughness of the metallic electrode surface.

The findings obtained by an interdisciplinary approach, between materials science and electrochemistry, represent preliminary researches, and further studies need in order to elucidate the complex phenomena which take place.

Author Contributions: Conceptualization, R.B., C.I.F., G.L.T. and L.B.; methodology, C.I.F., G.L.T. and L.B.; writing—original draft preparation, C.I.F., G.L.T. and L.B.; writing—review and editing, R.B., G.L.T. and L.B.; visualization, R.B.; supervision, R.B. All authors have read and agreed to the published version of the manuscript.

Funding: This research received no external funding.

Acknowledgments: This work was supported by a grant of the Romanian National Authority for Scientific Reasearch CNCS-UEFISCDI, project number PN-III-P2-2.1-PED-2019-3664 (R.B. and L.B.). Authors would also like to thank Lucian Barbu-Tudoran for SEM/EDS experiments.

Conflicts of Interest: The authors declare no conflict of interest.

References

1. Bronzino, J.D.; Peterson, D.R. The Biomedical Engineering Handbook, 4th ed.CRC Press: Boca Raton, FL, USA, 2015.
2. Calandrelli, L.; Immirzi, B.; Malinconicon, M.; Luessenheide, S.; Passaro, I.; Pasquale, R.; Oliva, A. Natural and synthetic hydroxyapatite filled PCL: mechanical properties and biocompatibility analysis. *J. Bioact. Compat. Polym.* **2004**, *19*, 301–313. [CrossRef]
3. Al Bahrawy, M. Hydroxyapatite as a Biomaterial to Improve Stem Cell-Related Tissue Engineering. *Biomed. J. Sci. Tech. Res.* **2020**, *25*, 19209–19226.
4. Hench, L.L. Bioceramics: From Concept to Clinic. *J. Am. Ceram. Soc.* **1991**, *74*, 1487–1510. [CrossRef]
5. Aoki, H. *Science and Medical Applications of Hydroxyapatite*; Japanese Association of Apatite Science: Tokyo, Japan, 1991.
6. Suchanek, W.; Masahiro, Y. Processing and properties of hydroxyapatite-based biomaterials for use as hard tissue replacement implants. *J. Mater. Res.* **1998**, *13*, 94–117. [CrossRef]
7. Bonfield, W.; Best, S.; Krajewski, A.; Ravaglioli, A. Prospects for Ceramics In Clinical Applications. In Proceedings of the Fourth EuroCeramics, Riccione, Italy, 2–6 October 1995.
8. Hench, L.L. *Ceramics and Society, Discussions of the Academy of Ceramics Forum '92, Assisi, Italy*. edited by R. J. Brook. 1995. Available online: http://www.waceramics.org/Forum92.pdf (accessed on 17 December 2020).
9. Wüsterfeld, M.; de Groot, K. Patent literature as a source of information for research and development: An investigation on calcium phosphate-containing biomaterials, part I. *J. Biomed. Mater. Res. Appl. Biomater.* **1989**, *23*, 41–71. [CrossRef] [PubMed]
10. Wilson, J. Special Report-World Biomaterials Congresses 1980–1992. *J. Appl. Biomater.* **1993**, 103–105. [CrossRef]
11. Ayadi, I.; Ayed, F.B. Mechanical optimization of the composite biomaterial based on the tricalcium phosphate, titania and magnesium fluoride. *J. Mech. Behav. Biomed.* **2016**, *60*, 568–580. [CrossRef]
12. Sivaperumal, V.R.; Mani, R.; Nachiappan, M.; Arumugam, K. Direct hydrothermal synthesis of hydroxyapatite/alumina nanocomposite. *Mater. Charact.* **2017**, *134*, 416–421. [CrossRef]
13. Arifta, T.I.; Munar, M.L.; Tsuru, K.; Ishikawa, K. Fabrication of interconnected porous calcium-deficient hydroxyapatite using the setting reaction of α tricalcium phosphate spherical granules. *Ceram. Int.* **2017**, *43*, 11149–11155. [CrossRef]
14. Guidara, A.; Chaari, K.; Fakhfakh, S.; Bouaziz, J. The effects of MgO, ZrO_2 and TiO_2 as additives on microstructure and mechanical properties of Al_2O_3-Fap composite. *Mater. Chem. Phys.* **2017**, *202*, 358–368. [CrossRef]

15. Jun, Y.-K.; Kim, W.H.; Kweon, O.-K.; Hong, S.-H. The fabrication and biochemical evaluation of alumina reinforced calcium phosphate porous implants. *Biomaterials* **2003**, *24*, 3731–3739. [CrossRef]
16. Fernandes, K.R.; Zhang, Y.; Magri, A.M.P.; Renno, A.C.M.; van den Beucken, J.J.J.P. Biomaterial Property Effects on Platelets and Macrophages: An in Vitro Study. *ACS Biomater. Sci. Eng. C* **2017**, *3*, 3318–3327. [CrossRef] [PubMed]
17. Shariff, K.A.; Tsuru, K.; Ishikawa, K. Fabrication of dicalcium phosphate dihydrate-coated beta-TCP granules and evaluation of their osteoconductivity using experimental rats. *Mater. Sci. Eng.* **2017**, *75*, 1411–1419. [CrossRef]
18. Oh, K.J.; Ko, Y.B.; Whang, I.C.; Jaiswa, L.S. Comparison of osteoconductivity and absorbability of beta-tricalcium phosphate and hydroxyapatite in clinical scenario of opening wedge high tibial osteotomy. *J. Mater. Sci. Mater. Med.* **2016**, *27*, 3318–3327.
19. French, R.H.; Glass, S.J.; Ohuchi, F.S.; Xu, Y.-N.; Ching, W.Y. Experimental and theoretical determination of the electronic structure and optical properties of three phases of ZrO_2. *Phys. Rev. B.* **1994**, *49*, 5133–5142. [CrossRef]
20. Goff, J.P.; Hayes, W.; Hull, S.; Hutchings, M.T.; Clausen, K.N. Defect structure of yttria-stabilized zirconia and its influence on the ionic conductivity at elevated temperatures. *Phys. Rev. B.* **1999**, *59*, 14202–14219. [CrossRef]
21. Denry, I.; Kelly, J.R. State of the art of zirconia for dental applications. *Dent. Mater.* **2008**, *24*, 299–307.
22. Gupta, T.K.; Lange, F.F.; Bechtold, J.H. Effect of stress-induced phase transformation on the properties of polycrystalline zirconia containing metastable tetragonal phase. *J. Mater. Sci.* **1978**, *13*, 1464–1470. [CrossRef]
23. Nath, S.; Baja, S.; Basu, B. Microwave-Sintered MgO-doped zirconia with improved mechanical and tribological properties. *Int. J. Appl. Ceram. Technol.* **2008**, *5*, 49–62. [CrossRef]
24. Rao, Y.; Wang, W.; Tan, F.; Chi, Y.; Lu, J.; Qiao, X. Influence of different ions doping on the antibacterial properties of MgO nanopowders. *Appl. Surf. Sci.* **2013**, *284*, 726–731. [CrossRef]
25. Noori, A.J.; Kareem, F.A. The effect of magnesium oxide nanoparticles on the antibacterial and antibiofilm properties of glass-ionomer cement. *Heliyon* **2019**, *5*, 1–7. [CrossRef] [PubMed]
26. Nguyen, N.T.; Grelling, N.; Wetteland, C.L.; Rosario, R.; Liu, H. Antimicrobial Activities and Mechanisms of Magnesium Oxide Nanoparticles (nMgO) against Pathogenic Bacteria, Yeasts, and Biofilms. *Sci. Rep.* **2018**, *8*, 1–23. [CrossRef]
27. Tang, Z.-X.; Bin-Feng, L. MgO nanoparticles as antibacterial agent: preparation and activity. *Braz. J. Chem. Eng.* **2014**, *31*, 591–601. [CrossRef]
28. Rapacz-Kmita, A.; Slósarczyk, A.; Paszkiewicz, Z. Mechanical properties of HAp–ZrO_2 composites. *J. Eur. Ceram. Soc.* **2006**, *26*, 1481–1488. [CrossRef]
29. Antoniac, I. Bioceramics and Biocomposites: From Research to Clinical Practice. Wiley-VCH: Weinheim, Germany, 2019.
30. Ziębowicz, A.; Matus, K.; Pakieła, W.; Matula, G.; Pawlyta, M. Comparison of the Crystal Structure and Wear Resistance of Co-Based Alloys with Low Carbon Content Manufactured by Selective Laser Sintering and Powder Injection Molding. *Crystals* **2020**, *10*, 197. [CrossRef]
31. Turdean, G.L.; Craciun, A.; Popa, D.; Constantiniuc, M. Study of electrochemical corrosion of biocompatible Co–Cr and Ni–Cr dental alloys in artificial saliva. Influence of pH of the solution. *Mater. Chem. Phys.* **2019**, *233*, 390–398. [CrossRef]
32. de Sá, J.; Vieira, F.; Aroso, C.M.; Cardoso, M.; Mendes, J.M.; Silva, A.S. The Influence of Saliva pH on the Fracture Resistance of Three Complete Denture Base Acrylic Resins. *Int. J. Dent.* **2020**, 1–12. [CrossRef]
33. Barabás, R.; Czikó, M.; Dékány, I.; Bizo, L.; Bogya, E.S. Comparative study of particle size analysis of hydroxyapatite-based nanomaterials. *Chem. Pap.* **2013**, *67*, 1414–1423. [CrossRef]
34. Barabás, R.; de Souza Ávila, E.; Ladeira, L.O.; Mosqueira Antônio, L.; Tötös, R.; Simedru, D.; Bizo, L.; Cadar, O. Graphene Oxides/Carbon Nanotubes–Hydroxyapatite Nanocomposites for Biomedical Applications. *Arab. J. Sci. Eng.* **2020**, *45*, 219–227. [CrossRef]
35. Barabás, R.; Deemter, D.; Katona, G.; Batin, G.; Barabás, L.; Bizo, L.; Cadar, O. Comparative study on physicochemical and mechanical characterization of new nanocarbon-based hydroxyapatite nanocomposites. *Turk. J. Chem.* **2019**, *43*, 809–824. [CrossRef]
36. Bizo, L.; Sabo, K.; Barábas, R.; Katona, G.; Barbu-Tudoran, L.; Berar, A. Structural, morphological and dissolution properties of ZrO_2-based biocomposites for dental applications. *Studia UBB Chemia* **2020**, *1*, 137–148. [CrossRef]
37. de Queiroz, G.M.O.; Silva, L.F.; Lima Ferreira, J.T.; da Cunha, J.A.; Gomes, P. Sathler, Electrochemical behavior and pH stability of artificial salivas for corrosion tests. *Braz. Oral Res.* **2007**, *21*, 209–215. [CrossRef] [PubMed]
38. Močnik, P.; Kosec, T.; Kovač, J.; Bizjak, M. The effect of pH, fluoride and tribocorrosion on the surface properties of dental archwires. *Mater. Sci. Eng. C* **2017**, *78*, 682–689. [CrossRef] [PubMed]
39. Salehi, S.; Fathi, M.H. Fabrication and characterization of sol-gel derived hydroxyapatite/zirconia composite nanopowders with various yttria contents. *Ceram. Int.* **2010**, *36*, 1659–1667. [CrossRef]
40. Lukić, M.J.; Veselinović, L.; Stevanović, M.; Nunić, J.; Dražič, G.; Marković, S.; Uskoković, D. Hydroxyapatite nanopowders prepared in the presence of zirconium ions. *Mater. Lett.* **2014**, *122*, 296–300. [CrossRef]
41. Patterson, A.L. The Scherrer Formula for X-Ray Particle Size Determination. *Phys. Rev.* **1939**, *56*, 978–982. [CrossRef]
42. Porojan, L.; Savencu, C.E.; Costea, L.V.; Dan, M.L.; Porojan, S.D. Corrosion Behavior of Ni-Cr Dental Casting Alloys. *Int. J. Electrochem. Sci.* **2018**, *13*, 410–423.
43. Murray, J.N. Electrochemical test methods for evaluating organic coatings on metals: an update. Part II: single test parameter measurements. *Prog. Org. Coat.* **1997**, *31*, 255–264. [CrossRef]

44. Rodríguez-Díaz, R.A.; Ramirez-Ledesma, A.L.; Aguilar-Mendez, M.A.; Uruchurtu Chavarin, J.; Hernández Gallego, M.A.; Juarez-Islas, J.A. Electrochemical corrosion behavior of a Co20Cr alloy in artificial saliva. *Int. J. Electrochem. Sci.* **2015**, *10*, 7212–7226.
45. Talha, M.; Ma, Y.; Kumar, P.; Lin, Y.; Singh, A. Role of protein adsorption in the bio corrosion of metallic implants - A review. *Colloids Surf. B Biointerfaces* **2019**, *176*, 494–506. [PubMed]
46. Bard, A.J.; Faulkner, L.R. Electrochemical Methods. Fundamentals and Applications. Wiley-VCH: Weinheim, Germany, 2001.
47. Brett, C.M.A.; Oliveira Brett, A.M. Electrochemistry: Principles, Methods, and Applications. Oxford University Press: Oxford, UK, 1994.
48. Du, J.; Ying, Y.; Guo, X.-Y.; Li, C.; Wu, Y.; Wen, Y.; Yang, H.-F. Acetohydroxamic acid adsorbed at copper surface: electrochemical, Raman and theoretical observations. *Int. J. Ind. Chem.* **2017**, *8*, 285–296. [CrossRef]
49. Fort, I.C.; Turdean, G.L.; Barabas, R.; Popa, D.; Ispas, A.; Constantiniuc, M. Study of the hydrogen peroxide based whitening gel on the corrosion of dental metallic alloys. *Studia UBB Chemia* **2019**, *64*, 125–133. [CrossRef]
50. Li, S.; Zhao, C.; Gou, H.; Li, Y.; He, X.; Zhao, L. Advanced anticorrosion coatings prepared from polybenzoxazine/α-zirconium phosphate nanocomposites. *Int. J. Electrochem. Sci.* **2018**, *13*, 2661–2675. [CrossRef]
51. Hsu, R.W.-W.; Yang, C.-C.; Huang, C.-A.; Chen, Y.-S. Electrochemical corrosion studies on Co–Cr–Mo implant alloy in biological solutions. *Mater. Chem. Phys.* **2005**, *93*, 531–538. [CrossRef]
52. Turdean, G.L.; Fort, I.C.; Simon, V. In vitro short-time stability of a bioactive glass-chitosan composite coating evaluated by using electrochemical methods. *Electrochim. Acta* **2015**, *182*, 707–714. [CrossRef]